The Quasi-Equilibrium Longitudinal Profile in Backwater Reaches of the Engineered Alluvial River

A Space-Marching Method

Arkesteijn, Liselot; Blom, Astrid; Czapiga, Matthew J.; Chavarrías, Víctor; Labeur, Robert Jan

DOI
10.1029/2019JF005195

Publication date
2019

Document Version
Final published version

Published in
Journal of Geophysical Research: Earth Surface

Citation (APA)
Arkesteijn, L., Blom, A., Czapiga, M. J., Chavarrías, V., & Labeur, R. J. (2019). The Quasi-Equilibrium Longitudinal Profile in Backwater Reaches of the Engineered Alluvial River: A Space-Marching Method. *Journal of Geophysical Research: Earth Surface*, *124*(11), 2542-2560. https://doi.org/10.1029/2019JF005195

JGR Earth Surface

RESEARCH ARTICLE
10.1029/2019JF005195

Key Points:
- Quasi-equilibrium channel geometry is separated into two temporal scales with quasi-static (long-term) and dynamic (short-term) components
- Hydrograph effects are decoupled; the quasi-static component relies on the flow duration curve, but the dynamic one on the flow rate order
- The static slope approximation enables a rapid space-marching solution of quasi-equilibrium geometry in backwater reaches

Correspondence to:
A. Blom,
astrid.blom@tudelft.nl

Citation:
Arkesteijn, L., Blom, A., Czapiga, M. J., Chavarrías, V., & Labeur, R. J. (2019). The quasi-equilibrium longitudinal profile in backwater reaches of the engineered alluvial river: A space-marching method. *Journal of Geophysical Research: Earth Surface*, *124*. https://doi.org/10.1029/2019JF005195

Received 10 JUN 2019
Accepted 16 SEP 2019
Accepted article online 23 OCT 2019

The Quasi-Equilibrium Longitudinal Profile in Backwater Reaches of the Engineered Alluvial River: A Space-Marching Method

Liselot Arkesteijn[1], Astrid Blom[1], Matthew J. Czapiga[1], Víctor Chavarrías[1,2], and Robert Jan Labeur[1]

[1]Faculty of Civil Engineering and Geosciences, Delft University of Technology, Delft, Netherlands, [2]Now at Deltares, Delft, Netherlands

Abstract An engineered alluvial river (i.e., a fixed-width channel) has constrained planform but is free to adjust channel slope and bed surface texture. These features are subject to controls: the hydrograph, sediment flux, and downstream base level. If the controls are sustained (or change slowly relative to the timescale of channel response), the channel ultimately achieves an equilibrium (or quasi-equilibrium) state. For brevity, we use the term "quasi-equilibrium" as a shorthand for both states. This quasi-equilibrium state is characterized by quasi-static and dynamic components, which define the characteristic timescale at which the dynamics of bed level average out. Although analytical models of quasi-equilibrium channel geometry in quasi-normal flow segments exist, rapid methods for determining the quasi-equilibrium geometry in backwater-dominated segments are still lacking. We show that, irrespective of its dynamics, the bed slope of a backwater or quasi-normal flow segment can be approximated as quasi-static (i.e., the static slope approximation). This approximation enables us to derive a rapid numerical space-marching solution of the quasi-static component for quasi-equilibrium channel geometry in both backwater and quasi-normal flow segments. A space-marching method means that the solution is found by stepping through space without the necessity of computing the transient phase. An additional numerical time stepping model describes the dynamic component of the quasi-equilibrium channel geometry. Tests of the two models against a backwater-Exner model confirm their validity. Our analysis validates previous studies in showing that the flow duration curve determines the quasi-static equilibrium profile, whereas the flow rate sequence governs the dynamic fluctuations.

1. Introduction

The primary controls on channel characteristics in an alluvial river are the flow duration curve (i.e., magnitude of flow rates and their frequency of occurrence), the grain size-specific sediment flux, and the base level. Here channel characteristics reflect the channel slope, channel width, and the grain size distribution of the bed surface sediment (i.e., the bed surface texture). We distinguish between a wide range of timescales regarding changes in the controls; long timescales scale with changes in climate, land use, and large flood events, and shorter timescales are associated with the temporal variation in rates of precipitation, runoff, snow melt, and base level setup due to atmospheric storm systems.

A river reach tends toward equilibrium channel characteristics (Blom, Arkesteijn, et al., 2017; Gilbert, 1877; Lane, 1955; Mackin, 1948). It will eventually reach these characteristics if the controls are either sustained (i.e., equilibrium conditions) or change slowly relative to the timescale of channel response (i.e., quasi-equilibrium conditions). The equilibrium state changes with time if the controls are nonstationary. A static equilibrium state only forms under strictly constant controls (Figure 1a). Otherwise, under controls with fluctuations, the equilibrium state is characterized by fluctuations in bed level, slope, width, and surface texture (e.g., Blom, Arkesteijn, et al., 2017; Bolla Pittaluga et al., 2014; Viparelli et al., 2011; Wong & Parker, 2006); this is called a dynamic equilibrium state (Figure 1b). The latter has been labeled a "steady-state equilibrium" or "statistical equilibrium" (e.g., Chorley & Kennedy, 1971), "averaged equilibrium" (Bolla Pittaluga et al., 2015), a "dynamic equilibrium" (e.g., Ahnert, 1994; Blom, Arkesteijn, et al., 2017; De Vries, 1993; Zhou et al., 2017), and a "river in regime" or "at grade" (e.g., Gilbert, 1877; Mackin, 1948; Pickup & Rieger, 1979).

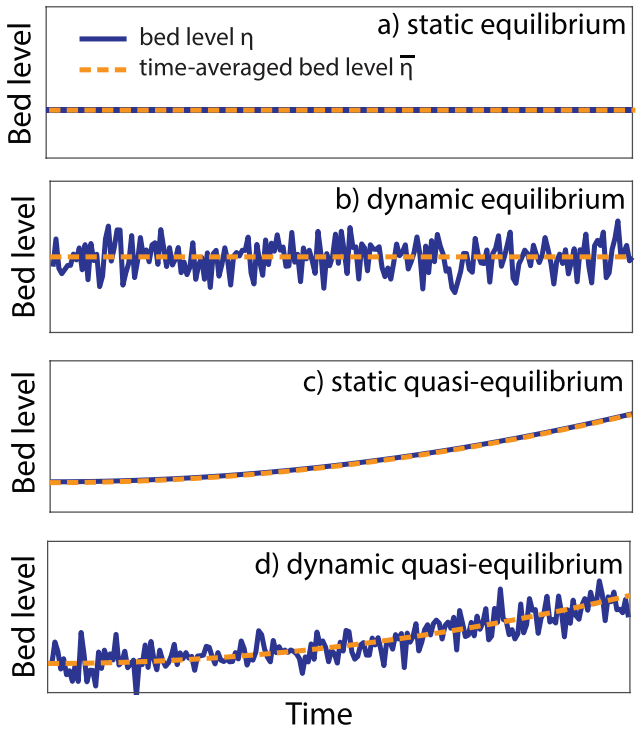

Figure 1. Schematics for different types of equilibria.

A dynamic equilibrium is achieved when the time-averaged sediment flux supplied from upstream is equal to the time-averaged sediment transport capacity, for each of the grain size fractions (e.g., Blom et al., 2016; Blom, Arkesteijn, et al., 2017; Mackin, 1948). This condition can be adjusted to account for particle abrasion (Blom et al., 2016), but the current analysis assumes unisize sediment and omits mixed-grain size and abrasion effects.

The channel response timescale or system relaxation time reflects how fast a reach responds (with respect to channel slope, channel width, and the bed surface texture) to changes in the controls (Blom et al., 2017; De Vries, 1975; Howard, 1982). As the channel response timescale is generally long, there exists a subset of relatively short-term control changes that do not appreciably affect the equilibrium state. This implies that short-term periodicity in controls produces negligible to limited associated channel response (e.g., Chatanantavet & Lamb, 2014; Howard, 1982; Viparelli et al., 2012). On the contrary, if the channel response timescale is much shorter than the timescale of changes of the controls (e.g., for slow control changes or in a small, highly mobile reach), channel geometry keeps pace with the changing controls (i.e., a quasi-equilibrium state; Figure 1c; Blom, Chavarrías, et al., 2017; Howard, 1982).

Variation of the controls over a short timescale only weakly perturbs these equilibrium characteristics, resulting in a state referred to as a dynamic quasi-equilibrium (Figure 1d). Under such conditions, the channel is governed by (dynamic) equilibrium conditions at all times. The fact that short-term quasi-periodicity in the hydrograph is not necessarily reflected in the channel slope allows us to assume that the channel slope is static over a short timescale, which we term the "static slope approximation." This approximation is essential to our analysis.

The characteristic timescale T is the timescale at which channel equilibrium regarding bed level is defined. At this timescale, by definition, the dynamics of the equilibrium longitudinal profile average out (i.e., short-term fluctuations in bed level and bed slope average out). For instance, the timescale T is much longer than the timescale of bed-level variations associated with bedform migration. Furthermore, the characteristic timescale T must be chosen short enough such that at that timescale the quasi-equilibrium state is maintained.

The definition of the characteristic timescale T separates quasi-equilibrium geometry into two components: the quasi-static component and the dynamic component. The former represents generalized channel geometry through averaging over the characteristic timescale T, and the latter includes all of the short-term (significantly less than T) fluctuations to bed elevation, slope, channel width, and surface texture from the quasi-static state.

A river reach can be classified into three longitudinal regions based on boundary condition effects: an upstream boundary segment (sometimes called hydrograph boundary layer), quasi-normal flow segment, and a backwater segment (Blom, Arkesteijn, et al., 2017), as illustrated in Figure 2. A backwater segment develops when base level deviates from the normal flow depth (under subcritical flow conditions). This segment is ubiquitous throughout a river; it develops upstream of the river mouth (e.g., Chatanantavet & Lamb, 2014; Chow, 1959; Lamb et al., 2012; Lane, 1957; Nittrouer et al., 2011, 2012), confluences (e.g., Meade et al., 1991), bifurcations, and locations with spatially varying channel width, slope, or friction. An upstream boundary segment (e.g., An, Cui, et al., 2017; An, Fu, et al., 2017; Parker, 2004b; Parker et al., 2008; Wong & Parker, 2006) forms when the instantaneous sediment supply rate does not match the instantaneous sediment transport capacity, despite equivalent time-averaged values. An upstream boundary segment develops downstream of confluences, bifurcations, and locations with spatially varying channel width, slope, or friction. The temporal mismatch leads to persistent downstream-migrating adjustment waves of bed elevation and surface texture that may dampen with downstream position (e.g., Parker et al., 2008). An upstream boundary segment and backwater segment may be present simultaneously. A quasi-normal flow segment forms where, despite the temporal variation of the flow rate, the flow is

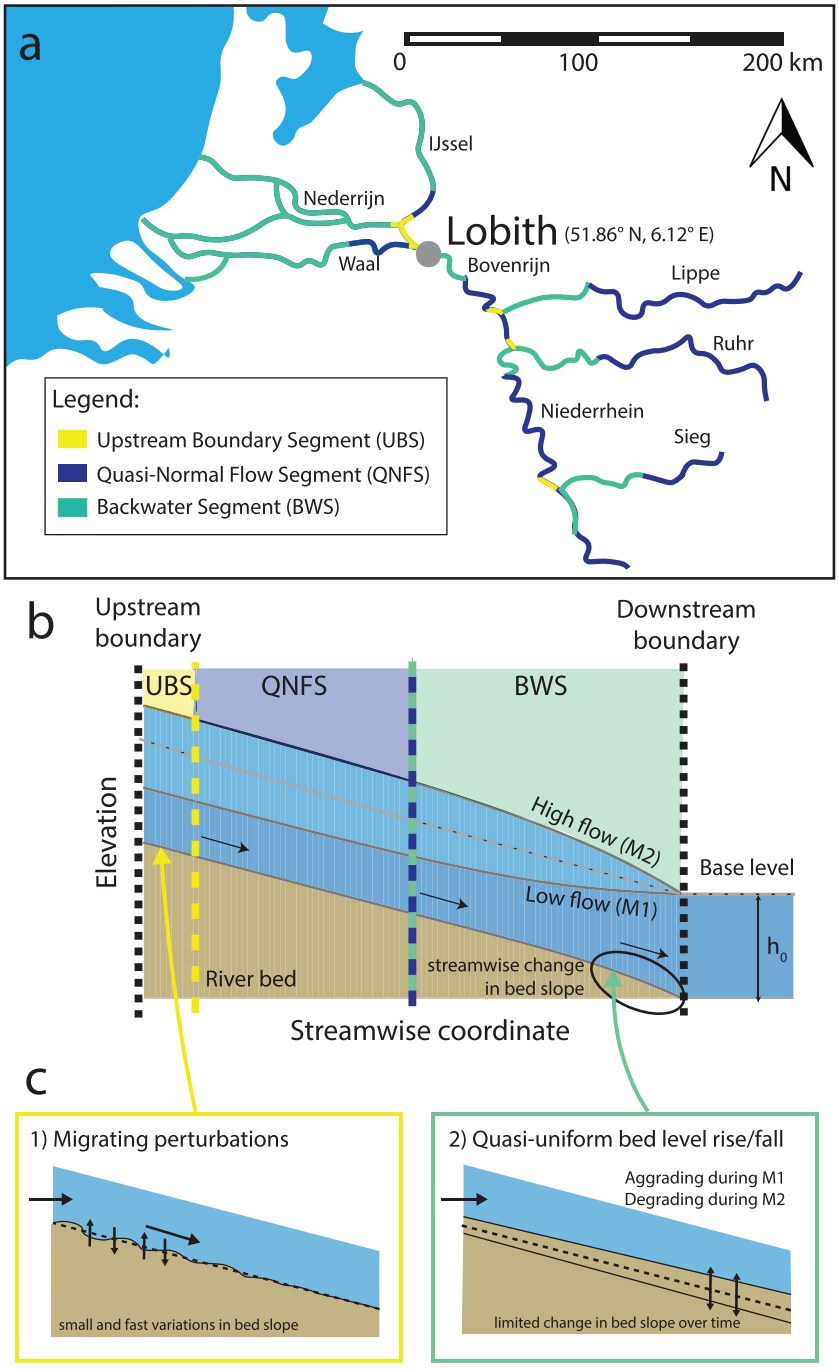

Figure 2. Schematic of the lower Rhine basin indicating (a) UBS, QNFS, and BWS; (b) a schematic of a river reach with each of the three characteristic segments; and (c) bed-level dynamics associated with variable flow in (1) an upstream boundary segment and (2) a backwater segment.

quasi-uniform at each flow rate (e.g., Lamb et al., 2012) and exists where backwater and upstream boundary effects are absent (Blom, Arkesteijn, et al., 2017; Chatanantavet & Lamb, 2014; Lane, 1955).

The notion of quasi-equilibrium has motivated development of models for quasi-equilibrium river geometry (see Blom, Arkesteijn, et al., 2017, for an overview). These models provide tools for rapid assessment of the quasi-equilibrium river geometry and the long-term river response to natural changes in controls and river training works (e.g., De Vriend, 2015). A limitation of these models is that they typically only apply to quasi-normal flow segments (e.g., Blom et al., 2016; Blom, Arkesteijn, et al., 2017; Blom, Chavarrías, et al.,

2017; De Vries, 1974) or conditions with a spatially variable channel width and a steady water discharge (Bolla Pittaluga et al., 2014; Li et al., 2014). As such, these models cannot be applied to backwater reaches, for example, upstream of a river mouth.

Our objective is to provide a method for assessing both equilibrium and quasi-equilibrium river geometry in backwater reaches. For brevity, we use the term "quasi-equilibrium" as a shorthand for both equilibrium and quasi-equilibrium cases. In particular, we derive two models: Model A describes the time-averaged or quasi-static component of the quasi-equilibrium river geometry and Model B its dynamic component. Our analysis is limited to engineered alluvial rivers, which are defined here as river reaches with fixed channel planform and width. This condition simplifies our analysis, as it implies that only one quasi-equilibrium state exists (Blom et al., 2016; Blom, Arkesteijn, et al., 2017), with exception to branches downstream from a river bifurcation (Schielen & Blom, 2018). For simplicity, we only consider temporal changes in the upstream controls and disregard exchange of water and sediment between the main channel and its floodplain. Our analysis provides a framework that can be extended to more complex river geometry, for example, spatially changing channel width, and cases with multiple variable controls in later studies.

This contribution is divided into eight sections. Section 2 details the elementary assumption of our analysis: the static slope approximation. Section 3 discusses simplifications of our analysis, and section 4 explains the flow model. In section 5, we derive a method for the assessment of the quasi-static component of quasi-equilibrium geometry in backwater and quasi-normal flow segments, and in section 6 a model for its dynamic component. In sections 7 and 8, we test the two models against a backwater-Exner (BWE) model.

2. The Static Slope Approximation

The characteristic timescale T [s] is the timescale at which short-term fluctuations in bed level, bed slope, channel width, and surface texture average out. The following requirements are necessary for T; it must be chosen (1) long enough to capture the statistics of bed elevation and filter out short-term fluctuations in bed level and (2) short enough to make sure quasi-equilibrium is maintained at that timescale. We distinguish between two components of bed level η [m], the quasi-static component $\overline{\eta}$ [m] and a dynamic or fluctuating component $\Delta\eta$ [m]:

$$\eta = \overline{\eta} + \Delta\eta, \tag{1}$$

with

$$\overline{\eta} = \frac{1}{T}\int_{t_0}^{t_0+T} \eta \ \mathrm{d}t, \tag{2}$$

and

$$\frac{1}{T}\int_{t_0}^{t_0+T} \Delta\ \eta \ \mathrm{d}t = 0, \tag{3}$$

where t [s] denotes time, t_0 [s] is an arbitrary starting time, and $\overline{\eta}$ is the average elevation over timescale T. In general, the bar indicates the temporal average of the specific variable over characteristic timescale T.

We now hypothesize that the flow can be approximated with sufficient accuracy by neglecting bed slope fluctuations, ΔS [-], relative to the time-averaged or quasi-static bed slope, $\overline{S}$ [-] (where $S = \overline{S} + \Delta S$ and $S = -d\eta/ds$, with s [m] the streamwise coordinate). We use the term static slope approximation to describe our assumption that hydraulics can be modeled based on the quasi-static slope $\overline{S}$, rather than the instantaneous bed slope S [-].

The argumentation for the static slope approximation differs between the quasi-normal flow segment, backwater segment, and upstream boundary segment. In a quasi-normal flow segment, the spatial gradient in the flow velocity is negligible, by definition, which implies that significant bed-level fluctuations are absent and the static slope approximation holds.

An upstream boundary segment is characterized by perturbations migrating in the downstream direction. Propagation (and dampening) of these perturbations result from the effect of bed-level variations over the short timescale on the sediment transport rate. These short-term fluctuations are not accounted for when using the static slope approximation.

In a backwater segment, short-term fluctuations of bed level and slope result from alternating gradually varied flow conditions (i.e., alternating M1 and M2 profiles) and the associated spatial gradients in the sediment transport rate (e.g., Chatanantavet & Lamb, 2014; Chatanantavet et al., 2012; Ganti et al., 2016; Lamb et al., 2012; Lane, 1957; Nittrouer et al., 2012), which is illustrated in Figure 2b. Assuming a fairly constant base level, high flows produce an M2 backwater curve characterized by streamwise flow acceleration and bed degradation, while low flows form an M1 backwater curve with streamwise flow deceleration and bed aggradation (Chatanantavet & Lamb, 2014; Chatanantavet et al., 2012; Lane, 1957). Bed level and surface texture adjust following changes to flow rate. Although the bed level fluctuates over the short timescale, the change is rather uniform over the backwater domain (Figure 2c). Consequently, short-term changes of the channel bed slope are considered negligible. For this reason, the nonuniform flow affects the local flow depth much more strongly than the short-term bed-level fluctuations, and the static slope approximation is expected to be valid in a backwater segment.

We will test the validity of the static slope approximation regarding the quasi-static component of the quasi-equilibrium geometry in section 7 and the dynamic component in section 8. We will limit the analysis to the backwater segment and the quasi-normal flow segment. Before describing the channel quasi-equilibrium state, we discuss assumptions of our analysis and the flow model.

3. Simplifications and Assumptions

Our modeling effort is a strongly simplified one, as we aim to derive the simplest model representing the fundamental physics of the problem (Paola & Leeder, 2011). We consider cases for which the characteristic timescale T exists. Additionally, we limited our analysis to the following:

- an engineered alluvial channel with uniform and fixed channel width;
- a channel with a rectangular cross section and without floodplains;
- subcritical flow conditions;
- unisize sediment (therefore neither particle abrasion nor size-selective transport);
- bed-material load only (i.e., bed load as well as suspended bed-material load; Church, 2006; Paola, 2001);
- sediment is transported at capacity (i.e., we neglect the spatial and temporal lag of the sediment transport rate to capacity e.g., Phillips & Sutherland, 1989);
- reaches between confluences for which the statistics of the controls are known (i.e., no lateral inflow or extraction of water and sediment along the reach);
- cases with negligible bedform-related drag and constant values of bed friction and porosity of the bed sediment;
- a relatively wide channel (i.e., the hydraulic radius approaches the flow depth); and
- cases where subsidence or uplift, delta outbuilding, and sea level change are negligible or proceed so slowly that quasi-equilibrium conditions hold at all times.

These simplifications are not expected to affect the main conclusions of the present analysis and can be relaxed in future studies. Some simplifications will be addressed in section 9.

4. The Flow Model

Our analysis is limited to the channel response to temporal change of the upstream controls, particularly the flow rate. As a flood wave propagates downstream, it diffuses and lengthens. Here, we assume that flood wave propagation is instantaneous. Thus, although we do account for the temporal variability of the flow rate, we disregard the dynamics of a flood wave (Barneveld, 1988). As such, temporal variability of the flow rate is considered as a sequence of steady, gradually varied flow profiles (i.e., the "quasi-steady flow approximation"). In other words, we assume that flow conditions are quasi-steady (e.g., Cao & Carling, 2002; De Vries, 1965) or alternating steady (Blom, Arkesteijn, et al., 2017).

This, combined with the absence of lateral inflow nor extraction of water, implies that water discharge is uniform in the model domain. As such, the backwater equation (i.e., steady, one-dimensional Saint-Venant equations, e.g., Chow, 1959; Parker, 2004a) is applied for each value along the hydrograph (e.g., Bolla Pittaluga et al., 2014; Chow, 1959). We apply the static slope approximation to the backwater equation by exchanging the instantaneous channel bed slope S with the static or slowly varying channel slope $\overline{S}$

(section 2):

$$\frac{\mathrm{d}h}{\mathrm{d}s} = \frac{\overline{S} - S_f}{1 - \mathrm{Fr}^2}, \tag{4}$$

where

$$\overline{S} = \frac{1}{T}\int_{t_0}^{t_0+T} S\mathrm{d}t. \tag{5}$$

In equations (4) and (5), h [m] denotes flow depth, S_f [-] the friction slope, defined as $S_f = c_f \mathrm{Fr}^2$, with c_f [-] a dimensionless friction constant, $\mathrm{Fr} = u/\sqrt{gh}$ [-] the Froude number, u [m/s] the mean flow velocity, and $g = 9.81$ m/s^2 is the acceleration due to gravity.

5. Model A: The Quasi-Static Component of the Quasi-Equilibrium State

This section details the derivation of Model A for the quasi-static component of the quasi-equilibrium river geometry. To this end, we combine the flow model in equation (4) with the Exner (1920) equation, which describes the conservation of bed sediment mass. The sediment transport rate follows from a closure relation (e.g., Engelund & Hansen, 1967; Meyer-Peter & Müller, 1948; Wilcock & Crowe, 2003). As such, the sediment transport rate per unit width, q_b [m^2/s], is a function of the bed friction, grain size, and flow variables.

We modify the Exner equation using the backwater equation in equation (4), which is described in Appendix A:

$$\frac{\partial \eta}{\partial t} = \lambda(\overline{S} - S_f), \tag{6}$$

where λ [m/s] denotes the De Vries (1965) characteristic celerity of bed elevation change (i.e., the "bed celerity"), which indicates the speed at which a perturbation in bed elevation of infinitesimal height (for instance, a sediment hump of infinitesimal height) propagates:

$$\lambda = \frac{1}{1-p}\frac{1}{1-\mathrm{Fr}^2}\frac{u}{h}\frac{\partial q_b}{\partial u}, \tag{7}$$

where p [-] is the porosity of the bed sediment.

We average equation (6) over the characteristic timescale T to derive a formulation for the time rate of change of the quasi-static bed level, $\overline{\eta}$ (i.e., at the long timescale). To this end, we combine equation (6) with $\eta = \overline{\eta} + \Delta\eta$, average the resulting equation over the characteristic timescale T, and simplify the resulting equation as, by definition, $\overline{\Delta\eta} = 0$ and $\overline{\lambda}\,\overline{S} = \overline{\lambda}\,\overline{S}$ (as $\overline{S}$ is constant over the period T):

$$\frac{\partial \overline{\eta}}{\partial t} = \overline{\lambda}\,\overline{S} - \overline{\lambda S_f}. \tag{8}$$

Under equilibrium conditions, there is no change in bed level at the long timescale, that is, $\partial\overline{\eta}/\partial t = 0$. Under quasi-equilibrium conditions, the left-hand term of equation (8) is, by definition, very small compared to the right-hand terms and does not affect the quasi-equilibrium geometry. This implies that under equilibrium and quasi-equilibrium conditions, equation (8) simplifies to

$$\overline{S} = \frac{\overline{\lambda S_f}}{\overline{\lambda}}, \tag{9}$$

which provides a definition of the quasi-static component of the equilibrium channel bed slope. We term equation (9) the "bed slope equation". It illustrates that the quasi-static channel bed slope is a weighted time average of the friction slope, where the weighting factor is the bed celerity under a specific flow rate. The weighting factor or bed celerity can be considered an estimate of the morphodynamic activity under that flow rate (Wolman & Miller, 1960).

The bed slope equation in equation (9) is a first-order ordinary differential equation for the quasi-static component of the bed level. A necessary and sufficient boundary condition to solve it (Appendix B) is the quasi-static component of the bed level at the downstream end of the reach, $\overline{\eta}_L$, where L indicates the downstream end of the reach of interest.

Model A combines the backwater equation, equation (4), and appropriate hydrodynamic boundary conditions, with the bed slope equation, equation (9), and the boundary condition for $\overline{\eta}_L$ in equation (B5). As such, it solves for the quasi-static equilibrium profile, averaged over the characteristic timescale T. The mathematical structure of Model A enables a highly efficient numerical solution method, which is detailed in Appendix C.

6. Model B: The Dynamic Component of the Quasi-Equilibrium State

This section describes the derivation of Model B for the dynamic component of the quasi-equilibrium state of a river reach. Model B builds upon the solution of the quasi-static equilibrium profile described by Model A.

Model B applies the modified Exner formulation of equation (6) with $\eta = \overline{\eta} + \Delta\eta$ to the short timescale, where the quasi-static bed elevation, $\overline{\eta}$, does not vary at the short timescale ($\partial\overline{\eta}/\partial t = 0$):

$$\frac{\partial \Delta\eta}{\partial t} = \lambda(\overline{S} - S_f), \tag{10}$$

where both the bed celerity λ and friction slope S_f depend on time and follow from Model A, in particular the solution of the backwater equation in equation (4), and do not depend on $\Delta\eta$.

Equation (10) is an ordinary differential equation in time describing the dynamic component of the quasi-equilibrium state. Appendix D illustrates that equation (3) replaces the need for an initial condition and details the numerical solution of Model B.

7. Test of Model A

In this section we test Model A with particular focus on the static slope approximation. To this end, we compare the results of Model A to a time-marching backwater-Exner (BWE) model. We consider a highly schematic case, with temporally varying upstream controls; the constant base level at the river mouth sets backwater conditions (Figure 2b).

We use input parameters that roughly scale to the Waal branch of the Rhine River. We consider a 150-km single-branched reach with uniform channel width of 300 m. We select the bed load transport relation of Meyer-Peter and Müller (1948), a value for porosity of bed sediment, p, equal to 0.4, and the friction coefficient c_f equal to 0.007, which is a reasonable value for the Waal River (e.g., Paarlberg et al., 2008).

We use the 20th century hydrograph measured at Lobith, which is located along the Rhine River at the border between Germany and the Netherlands. We multiply the record by 2/3, as approximately 2/3 of the water discharge at Lobith flows through the Waal branch of the Rhine River (Figure 3a). We reduce the hydrograph record to a frequency of one data point every 5 days. In addition to the 100-year hydrograph, we subdivide the full hydrograph into five additional 20-year hydrographs, providing six in total, to provide insight on how differences between hydrographs affect equilibrium channel geometry. The mean flow rate is approximately 1,500 m^3/s, the mean annual peak flow rate is approximately 4,100 m^3/s, and peak flow rates are up to 8,000 m^3/s (Table 1).

Mean flow rate, mean annual peak flow rate, and extreme peak flow rates slightly vary among the six hydrographs, but the flow duration curves are all similar (Figure 3b). Differences in flow duration curves are only particularly noticeable in the tails, which represent peak events. In other words, frequency and regularity of peak flows vary between the hydrographs. Application of Model A to each hydrograph helps explain how differences between flow duration curves and regularity of peak flows affect the equilibrium state.

We cycle (i.e., periodically repeat) the six hydrographs (Ackers & Charlton, 1970), as this guarantees the existence of an equilibrium state. In fact, cycling a hydrograph makes a periodic equilibrium state (e.g., Bolla Pittaluga et al., 2015), where the period is equal to the duration of the hydrograph. Characteristic timescale T may be considered equal to, or bound by, this period.

We select a 300-km model domain, with a 150-km buffer region upstream of our 150-km-long domain of interest. The buffer region is sufficiently long such that the perturbations associated with an upstream boundary segment diffuse prior to reaching the domain of interest.

Based on field data analysis, the mean sediment flux into the Waal branch is estimated to be 0.62 Mt/year and consists of 90% of sand and 10% gravel (Frings et al., 2015). Here, we impose a sediment flux of 0.62 Mt/year

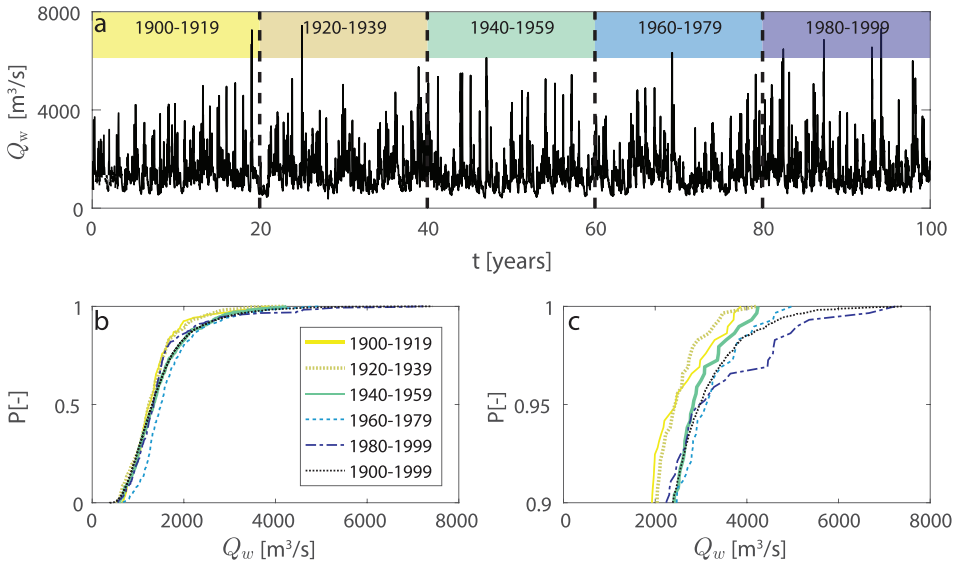

Figure 3. (a) The cycled 100-year hydrograph, or, alternatively, five cycled, consecutive 20-year hydrographs (with one discharge value every 5 days) of the Waal branch of the Rhine River; (b) flow duration curves for the six hydrographs, where Q_w [m^3/s] denotes the water discharge and P is the cumulative probability of the flow rate; and (c) the flow duration curves with a focus on peak flow rates. Water discharge values are equal to measured data of the Rhine River at Lobith, which is at the border between Germany and the Netherlands, multiplied by the factor 2/3 to adjust for flow in the Waal River.

and assume the sediment to be sand with a mean particle size of 1.3 mm. We impose the normal flow load distribution (i.e., the sedigraph of the quasi-normal flow segment Blom, Arkesteijn, et al., 2017) at the upstream end of the reach, since a measured time series of the sediment discharge is not available. Numerical settings of the model runs are listed in Appendix E.

The alternation of M1 and M2 backwater profiles affects the static component of the equilibrium channel slope in the backwater reach (Figure 4). Under conditions where the water discharge and channel width do not vary spatially and base level is constant, the channel bed slope increases with proximity to the mouth (i.e., a convex-upward profile), which confirms the studies by Lane (1957) and Lamb et al. (2012). The profile convexity can be understood from the following reasoning: in an end member case, where sediment becomes immobile at low flow near the basin due to an M1 backwater profile (Nittrouer et al., 2012), the period that sediment is actively transported shortens (compared to the upstream quasi-normal flow segment). The channel slope increases to enable transport of the sediment flux over the shorter time. This reasoning also holds under relaxed conditions that do not represent the above end member case; for instance, the M1-backwater condition at low flow reduces sediment mobility (compared to the upstream quasi-normal flow segment), which implies that the high flows must move a larger fraction content of the annual sediment flux. This leads to an increase of the channel slope with streamwise position.

Table 1
Characteristics of the 100-Year Hydrograph and Five 20-Year Hydrographs

Period	Flow rate (m^3/s)		Annual peak flow (m^3/s)	
	Mean	Standard deviation	Mean	Standard deviation
1900–1999	1,480	760	4,130	1,300
1900–1919	1,470	690	4,020	1,070
1920–1939	1,510	750	3,830	1,370
1940–1959	1,370	770	4,380	1,270
1960–1979	1,480	750	3,750	1,220
1980–1999	1,570	830	4,660	1,420

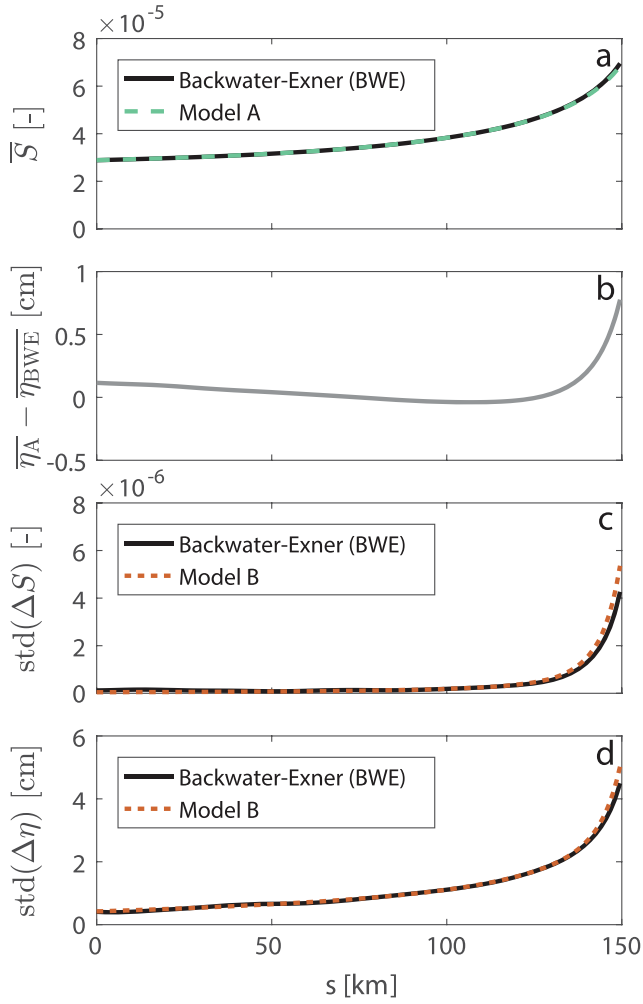

Figure 4. Validity of the static slope approximation: the quasi-static and dynamic components of the equilibrium river profile according to Models A and B compared against the time-marching backwater-Exner model: (a) the quasi-static component of the bed slope, (b) difference in the quasi-static component of the bed level between Model A in the BWE model, (c) standard deviation of the dynamic component of the bed slope, and (d) standard deviation of the dynamic component of the bed level. All results use the cycled 100-year hydrograph of Figure 3. In subfigures c and d, "std" refers to standard deviation.

The first test of Model A involves an assessment of whether its key assumptions are satisfied. The static slope approximation must hold for Model A to be valid. It does so if the short-term fluctuation of slope ΔS (here represented by its standard deviation) is small compared to the slowly varying slope $\overline{S}$. In our case, the quasi-static component of the equilibrium bed slope, $\overline{S}$ (Figure 4a), is at least a factor of 10 larger than the standard deviation of the dynamic component (Figure 4c). The second constraint is that short-term variation of bed level at the mouth is small compared to the flow depth at the mouth. In our case, the standard deviation of bed level at the mouth is approximately 0.05 m (Figure 4d), which is negligible compared to flow depth at the river mouth, h_L (almost 12 m).

We additionally test Model A by comparing results with a BWE model (Figure 4a). The maximum difference in predicted bed level between the two models occurs at the downstream boundary and is 0.8 cm (Figure 4b), which is negligible compared to the flow depth.

The above tests illustrate that Model A well predicts the static component of the equilibrium state, which confirms the validity of the static slope approximation in this case. Moreover, it implies that the quasi-static component of the quasi-equilibrium state depends on the flow duration curve and is unaffected by the flow rate sequence, which confirms the analysis by Chatanantavet et al. (2012).

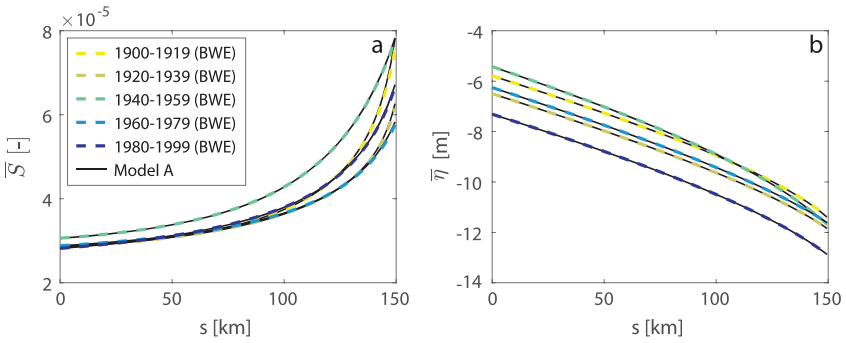

Figure 5. The quasi-static component of the quasi-equilibrium state according to Model A and the backwater-Exner model (BWE): (a) the quasi-static component of the bed slope and (b) the quasi-static component of the bed elevation. We consider the five cycled 20-year hydrographs of Figure 3.

Figure 5 shows the static component of the equilibrium state for the five cycled 20-year hydrographs. Model A performs well for all hydrographs, which again confirms the validity of the static slope approximation. The 1940–1959 hydrograph yields the largest static bed slope (Figure 5a). This is due to the lowest mean flow rate of all hydrographs (Table 1); for a smaller mean flow rate, the channel bed slope must be larger to transport the sediment flux downstream (Blom et al., 2016; Lane, 1955).

The static component of the bed slope at the upstream end of the reach (i.e., in the quasi-normal flow segment) does not vary strongly between the six hydrographs. Considering the differences in the tails of each flow duration curve (Figure 3c), this confirms that in a quasi-normal flow segment the equilibrium state depends mostly on the moderately high flows that carry the most sediment, rather than on peak flows that are stronger, but occur infrequently (e.g., Blom, Arkesteijn, et al., 2017; Lanzoni et al., 2015; Wolman & Miller, 1960).

The effect of peak flows on the quasi-static equilibrium geometry is more pronounced in the backwater segment than in the quasi-normal flow segment (Figure 5a). This can be attributed to an increased sediment transport rate associated with the M2 backwater during high flows and a decreased sediment transport rate associated with the M1 backwater during low flows, which increases the relative difference in the fraction content of the annual sediment flux between high and low flows.

The 1980–1999 hydrograph is characterized by four peak flow events above 6,000 m^3/s, whereas there was at most one peak flow of such magnitude in the other hydrographs. Therefore, the flow duration curve of 1980–1999 has a fatter tail than the other hydrographs. This results in a larger mean flow depth at the channel mouth (Chatanantavet & Lamb, 2014; De Vries, 1971), and, as a result, its equilibrium bed profile is established at a lower elevation (Figure 5b). Nevertheless, the fatter tail does not negatively affect the performance of Model A.

8. Test of Model B

Model B predicts the dynamic component of the equilibrium state. Figure 6 indicates that rare peak flows induce a sudden and large change in bed elevation (e.g., Bolla Pittaluga et al., 2014; Lamb et al., 2012; Lane, 1957). Quasi-periodicity of the bed level is associated with peak flows of a certain recurrence period, which in our case seems to be approximately 30 years.

We find that the relative importance of high flows and the associated bed-level fluctuations increase with proximity to the river mouth; this mirrors the results of Model A regarding the quasi-static component of the quasi-equilibrium geometry. This is, again, due to the increased relative difference in the fraction content of the annual sediment flux between high and low flows.

Results of Model B agree well with the time-marching BWE model (Figure 6), despite a slight overestimation of bed-level fluctuations at the mouth (on the order of 5 cm). Model B is based on the solution of the hydraulic variables associated with the quasi-static bed profile, whereas the time-marching BWE model accounts for changes of the hydraulic variables associated with the dynamic fluctuations of the bed profile. Understandably, the difference between the two models is largest when bed level deviates most from the static component of the equilibrium state (i.e., at the river mouth).

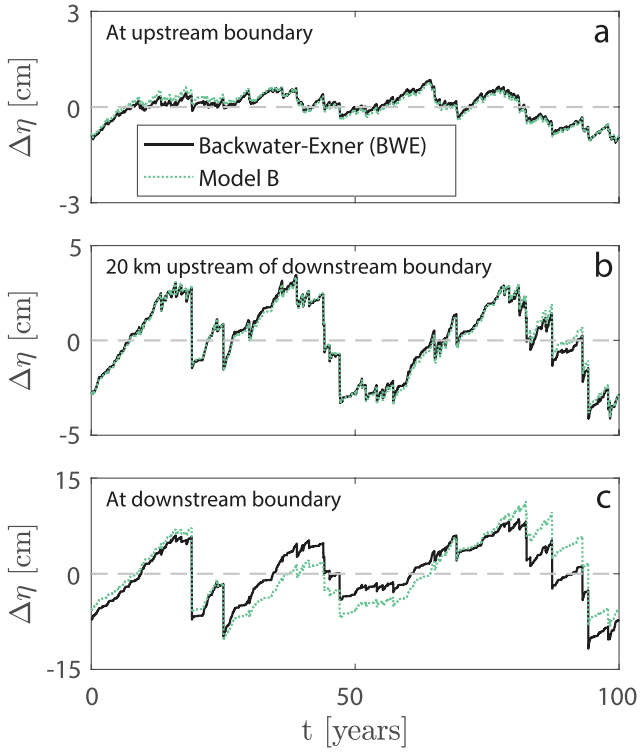

Figure 6. Short-term bed-level fluctuations as a function of time at (a) 150 km upstream of the mouth, (b) at 20 km upstream of the mouth, and (c) at the river mouth; results shown for the 100-year hydrograph.

Figure 7 shows the dynamic component of the quasi-equilibrium state at the river mouth for the five cycled 20-year hydrographs of Figure 5. Model B yields results that are very similar to the BWE model, which provides another confirmation regarding validity of the static slope approximation.

Results of the 1900–1919 hydrograph clearly differ from the other hydrographs. It shows continuous aggradation, except for one erosion event associated with a single-peak flow event. Peak flows, and their associated erosion events, are more evenly distributed over the other hydrographs, which lead to less dramatic changes in $\Delta\eta$.

The number of peak discharge events in the 1980–1999 hydrograph is relatively large. This is reflected in the static component of the equilibrium state through an increased flow depth and decreased bed elevation at the river mouth (Figure 5b). This increased flow depth reduces the importance of the M2 backwater effect and its associated erosion resulting from the peak flows. For this reason, single-peak flow events have a smaller effect on the dynamic component of the equilibrium state.

9. Discussion

The present analysis shows the time stepping BWE model of quasi-equilibrium geometry can be reproduced well with two much simpler models that separately address short-term fluctuations (Model B) and the time-averaged component (Model A) of quasi-equilibrium channel geometry. As such, our modeling framework provides a new space-marching method for determining the quasi-equilibrium channel geometry and the long-term river response to natural changes of the controls and river training measures (e.g., De Vriend, 2015). A space-marching solution method means that quasi-equilibrium channel geometry is solved from downstream to upstream without the necessity of computing the transient phase. The novelty of the method lies in its application to not only the quasi-normal flow segments, but also to backwater segments. Our results are also a proof of concept that (1) the traditional time stepping morphodynamic model can be time-split into quasi-static and dynamic components and (2) these separate models can be superimposed to reproduce similar results as the traditional method.

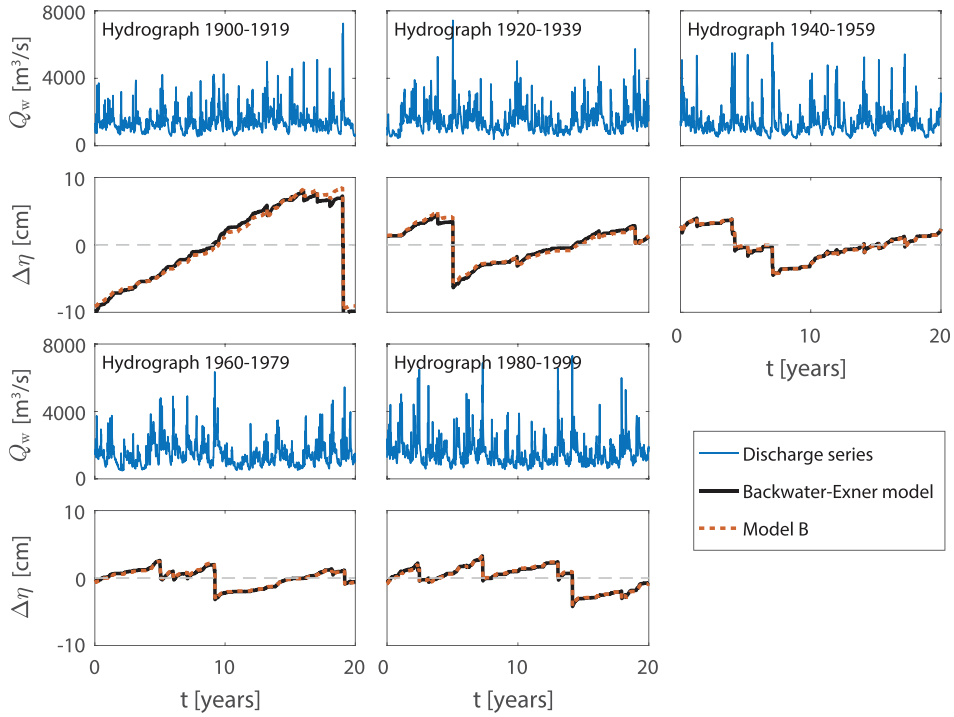

Figure 7. Results of the dynamic component of the quasi-equilibrium state represented by the fluctuation of bed elevation $\Delta\eta$, at the river mouth (where s is 150 km), according to Model B and the backwater-Exner model. We consider the five cycled 20-year hydrographs of Figure 3.

An additional outcome of our analysis illustrates how components of the given flow hydrograph affect the dynamic equilibrium state. Statistics of the hydrology, that is, the flow duration curve, only impact the quasi-static equilibrium, which represents a mean bed profile. Meanwhile, only the order of flow events affects the location and magnitude of fluctuations from quasi-static profile. As shown in section 6, the scale of bed fluctuations due to the sequence of flows includes a feedback mechanism that magnifies the dynamic bed elevation change. Therefore, as the time between peak flow events increases, we can expect a greater increase in the magnitude of dynamic bed elevation change both prior to (aggradation) and following (degradation) the high discharge event.

The computation time is dramatically reduced with this methodology. In our setup, numerical runs that take over 1 day with the BWE model can be achieved in seconds with the superimposed result of Models A and B. The speedup can be attributed to the model framework, which allows for a space-marching solution in place of explicit time stepping. For example, and to elaborate on the preceding point, this feature can now allow a robust Monte Carlo analysis regarding how flow order of a given flow duration curve affects the location and magnitude of short-term, dynamic bed elevation changes.

In our analysis we have considered a highly schematized alluvial channel with a temporally variable flow rate, a constant base level, and unisize sediment. The channel width is spatially and temporally constant, and specific deltaic features such as bifurcating branches are absent. Under such strongly idealized conditions, the alternating M1 and M2 backwater curves lead to a convex-upward profile. Aspects that make a field case such as the lower Mississippi River with its concave-upward profile (Nittrouer et al., 2012) different from our analysis here are, for instance, a spatially changing channel width, channel bifurcations, delta outbuilding, and mixed-size sediment:

- A streamwise decrease of the channel width induces a streamwise decrease of the equilibrium channel bed slope (Blom, Arkesteijn, et al., 2017), which implies a concave-upward profile. This is because a narrower channel is characterized by a larger equilibrium flow velocity, and, for that reason, a smaller channel slope suffices to transport the sediment flux downstream.
- Bifurcations in a delta lead to extraction of water and sediment from the trunk channel. If water and sediment are extracted without changing the ratio of the water and sediment discharge in the trunk channel,

the effect of water extraction dominates over sediment extraction. In that case the channel slope increases with streamwise position, leading to a convex-upward profile. A concave-upward profile may form in the trunk channel if sediment is extracted from the trunk channel with a larger fraction content than the water discharge.

- Delta outbuilding tends to decrease the slope with streamwise position and so strengthens concavity of the river profile (Sinha & Parker, 1996).
- Both particle abrasion and preferential deposition of coarse sediment lead to downstream fining and so strengthen concavity of the river profile (Blom et al., 2016).

Assumptions and simplifications embedded in the model limit its direct application to field cases. Many features can be added to a future version of the model. In our analysis, we have considered reaches with a highly schematized river planform, but the approach provides a framework that allows for more complex channel geometry in future analyses. These model extensions are discussed below.

Our framework assumes a spatially constant width. In reality, short-term variations in the flow rate lead to temporary deepening at narrow sections during high flows and gradual aggradation during low flows (Bolla Pittaluga et al., 2014; Ferrer-Boix et al., 2016).

The current analysis is limited to cases without floodplains. It is not trivial to include the effects of floodplains in the proposed method. There seem to be three possibilities: (1) to prescribe the difference in bed elevation between the main channel and the floodplains, (2) to prescribe the bed elevation of the floodplains, or (3) to account for the flux of water and sediment between the main channel and the floodplains (e.g., Lauer et al., 2016; Viparelli et al., 2013).

Addition of water and sediment to the trunk channel by tributaries has not been addressed in the present analysis. It can be accounted for provided that assumptions are made how the probability distribution of flow rates in the trunk channel is affected by the probability distribution or temporal variation of the flow rates in the tributaries.

It is not straightforward to account for distributaries or bifurcations using the proposed method. Multiple equilibrium states of channel geometry exist downstream of a bifurcation, which can be either stable or unstable (e.g., Schielen & Blom, 2018; Wang et al., 1995). In the case of multiple stable equilibrium states, the system initial condition determines which stable equilibrium configuration the system evolves toward (Schielen & Blom, 2018). The proposed method deals with neither multiple stable equilibrium states nor a dependence on the initial conditions.

We have shown that fluctuations of the controls lead to short-term fluctuations in bed level; these fluctuations of the controls also lead to changes in the channel bed surface texture. The present model uses a single grain size but can be amended to include mixed-size sediment, size-selective transport of sediment, and particle abrasion in a future study. Some of these features are currently added to an extended version of the model.

10. Conclusions

We define the characteristic timescale T of the quasi-equilibrium state of an engineered (i.e., fixed-width) alluvial reach as the one where the short-term fluctuations in bed level and channel slope average out. The definition of T implies that quasi-equilibrium channel geometry has two components. The quasi-static component is the channel geometry averaged over the timescale T. The dynamic component comprises fluctuations of bed elevation and channel slope around the quasi-static component. Here we model these components separately, then superimpose them, and create a result that agrees well with typical time-marching BWE models.

In a backwater reach, short-term variation of the water discharge moderately changes the bed level with negligible short-term changes of the channel bed slope. This suggests the channel slope is quasi-static (i.e., the static slope approximation).

The quasi-equilibrium channel slope appears as a weighted time average of the friction slope. The weighting factor is the bed celerity associated with a specific flow rate, which corresponds to the streamwise propagation celerity of an infinitesimal disturbance in bed elevation under the given flow rate. This weighting factor is representative of the morphodynamic work done under a certain flow rate.

The static slope approximation allows setup of a numerical space-marching model that enables assessment of the quasi-static component of quasi-equilibrium river geometry in backwater and quasi-normal flow segments. This space-marching model solves the quasi-equilibrium river geometry without solving for the transient phase. A second model, a time-marching numerical model, rapidly solves for the dynamic component of the quasi-equilibrium river geometry. We have successfully tested the two models against a traditional BWE model.

The flow duration curve (i.e., magnitude and frequency of flow rates) determines the quasi-static component of the quasi-equilibrium river geometry, and the latter is unaffected by the sequence of flood events, which confirms the analysis by Chatanantavet et al. (2012). The flow rate sequence does determine the dynamic component of the quasi-equilibrium river geometry.

A base level-induced backwater reach is characterized by a convex-upward profile (i.e., an increase of channel slope with streamwise position) in cases without (dis)tributaries and where channel width does not vary spatially. This matches with observations by Lamb et al. (2012). The long profile is convex-upward because high flows must allow for a higher fraction content of the annual sediment flux, as the M1-backwater profiles associated with low flows reduce sediment mobility (compared to the quasi-normal flow segment).

Application of the proposed method to a field case is still difficult, as the current version of the model does not account for a spatially changing channel width, mixed-size sediment, channel bifurcations, and delta outbuilding. As such, the traditional time-marching BWE model is the preferred tool in most field cases.

Appendix A: Alternative Exner Formulation

This appendix details the specifications of the derivation of equation (6),

$$\frac{\partial \eta}{\partial t} = \lambda(\overline{S} - S_f),$$

and equation (7),

$$\lambda = \frac{1}{1-p}\frac{1}{1-\mathrm{Fr}^2}\frac{u}{h}\frac{\partial q_b}{\partial u}.$$

Equation (6) was derived earlier using the Engelund and Hansen (1967) sediment transport relation (e.g., De Vries, 1974). Nevertheless, it also holds for other sediment transport relations, provided that the sediment transport rate depends on the flow velocity only (i.e., $q_b = f(u)$). This yields the following constraints: (a) the sediment transport rate per unit width, q_b, is a function of the shear stress, and (b) the friction coefficient does not depend on the local flow parameters.

Equations (6) and (7) follow from reworking the Exner equation for a channel with spatially constant width:

$$(1-p)\frac{\partial \eta}{\partial t} + \frac{\partial q_b}{\partial s} = 0, \tag{A1}$$

which yields

$$(1-p)\frac{\partial \eta}{\partial t} + \frac{\partial q_b}{\partial u}\frac{\partial u}{\partial s} = (1-p)\frac{\partial \eta}{\partial t} + \frac{\partial q_b}{\partial u}\frac{\partial Q_w/(Bh)}{\partial s} = 0, \tag{A2}$$

as $u = Q_w/(Bh)$, where Q_w [m^3/s] is the water discharge and B [m] the channel width. Elaboration of the second last term in equation (A2) yields

$$\frac{\partial q_b}{\partial u}\frac{\partial Q_w/(Bh)}{\partial s} = \frac{\partial q_b}{\partial u}\left(\frac{1}{Bh}\frac{\partial Q_w}{\partial s} - \frac{Q_w}{B^2h}\frac{\partial B}{\partial s} - \frac{Q_w}{Bh^2}\frac{\partial h}{\partial s}\right). \tag{A3}$$

Due to the quasi-steady flow assumption, the neglect of lateral inflow and outflow, and the uniform channel width, the gradients $\partial Q_w/\partial s$ and $\partial B/\partial s$ equal 0. As $Q_w/(h^2B) = u/h$, the Exner equation in equation (A2) reduces to

$$(1-p)\frac{\partial \eta}{\partial t} - \frac{u}{h}\frac{\partial q_b}{\partial u}\frac{\partial h}{\partial s} = 0. \tag{A4}$$

Combination of equations (A4) and (4) yields equations (6) and (7).

Appendix B: Boundary Condition for the Bed Slope Equation

A suitable boundary condition for the bed slope equation in equation (9) is derived from the boundary conditions of a typical time-marching BWE model. The latter generally consists of the following boundary conditions: (a) the hydrograph at the upstream end, Q_{w0} [m^3/s]; (b) the sedigraph at the upstream end, Q_{b0} [m^3/s]; and (c) the downstream water surface elevation or base level at $s = L$, η_{wL} [m]. Here we illustrate that by reworking the above boundary conditions, we obtain a formulation for the quasi-static component of the downstream bed elevation, $\overline{\eta}_L$, which varies at the long timescale only.

The sediment transport rate at the downstream boundary follows from a closure relation for the capacity-based sediment transport rate, $q_b = f(u)$, which can also be written as $q_b = f(Q_w, h, B)$:

$$Q_{bL} = B f(Q_{wL}, h_L, B). \tag{B1}$$

The flow depth at the downstream end, h_L, follows from

$$h_L = \eta_{wL} - \overline{\eta}_L - \Delta\eta_L, \tag{B2}$$

which is simplified to

$$h_L = \eta_{wL} - \overline{\eta}_L, \tag{B3}$$

assuming that the short-term bed-level fluctuations are small compared to the mean flow depth at the mouth (i.e., $\Delta\eta_L \ll \eta_{wL} - \overline{\eta}_L$). This assumption is justified by the simulation results in sections 7 and 8.

As a result of the quasi-steady flow approximation and absent lateral inflow or extraction of water, the water discharge at the downstream end of the reach, Q_{wL}, in equation (B1) equals the water discharge at the upstream end, Q_{w0}.

The time-averaged Exner equation tells us that, in a quasi-equilibrium state, the sediment transport averaged over the characteristic timescale T is constant along the reach (Blom et al., 2016; Mackin, 1948), provided that gravel abrasion (Blom et al., 2016) is disregarded along with lateral inflow or extraction of sediment along the reach:

$$\overline{\frac{\partial \eta}{\partial t}} \approx 0 \quad \Rightarrow \quad \overline{\frac{\partial Q_b}{\partial s}} \approx 0. \tag{B4}$$

As a result, the time-averaged sediment flux at the downstream end equals the time-averaged sediment supply to the reach: $\overline{Q_{bL}} = \overline{Q_{b0}}$.

Time-averaging of equation (B1) yields

$$\overline{Q_{b0}} = \overline{B f\left(Q_{w0}, \eta_{wL} - \overline{\eta}_L, B\right)}, \tag{B5}$$

from which we can solve the boundary condition for the quasi-static bed elevation at the downstream end of the reach, $\overline{\eta}_L$.

Appendix C: The Numerical Solution of Model A

The governing equations of Model A are listed in section 5. Here we describe how we numerically solve these equations.

The quasi-static component of the quasi-equilibrium state is described by the bed slope equation in equation (9), for which the boundary condition is provided in equation (B5). We approximate the time-averaged flow parameters in these equations using the backwater equation in equation (4).

We consider a characteristic timescale T that well represents the statistics of the bed-level fluctuations and define a time step Δt that provides a reasonable resolution of the changes in the controls (for instance, 1 day). A total number of K (where $K = T/\Delta t$) sets of boundary conditions ($Q_{w0}(t^j)$, $\eta_{wL}(t^j)$) are defined that indicate

the boundary conditions at time $t^j = t_0 + j\Delta t$, where $1 \leq j \leq K$. The backwater equation (equation (4)) is valid at all times t^j, leading to a system of K backwater equations that hold at time t^j:

$$\frac{\mathrm{d}h^j}{\mathrm{d}s} = \frac{\overline{S} - S_f^j}{1 - \mathrm{Fr}^{j2}}, \quad \text{given } \left(Q_{w0}(t^j), \eta_{wL}(t^j) - \overline{\eta}_L\right), \quad 1 \leq j \leq K. \tag{C1}$$

The notation h^j, S_f^j, and Fr^j indicates the fact that we consider K equations.

We write the bed slope equation in equation (9) and the downstream boundary condition in equation (B5) as a finite sum of the K flow rates as

$$\overline{S} = \frac{1}{K}\sum_{j=1}^{K}\left(\frac{1}{\frac{1}{K}\sum_{k=1}^{K}\lambda^k}\lambda^j S_f^j\right), \tag{C2}$$

$$\sum_{j=1}^{K} Q_{b0}(t^j) = \sum_{j=1}^{K} Bf\left(Q_{w0}(t^j), \eta_{wL}(t^j) - \overline{\eta}_L\right), \tag{C3}$$

where $1 \leq k \leq K$.

The combination of K backwater equations and one bed slope equation leads to a system of K+1 ordinary differential equations with the K values for flow depth and mean bed level as dependent variables. Appropriate boundary conditions are given by the K sets of hydrodynamic boundary conditions, and the description of $\overline{\eta}_L$ in equation (C3). The system of equations is solved by marching through space, starting from the downstream boundary, and numerically integrating the equations in upstream direction. Here we use the Euler Forward method, where we step through space in upstream direction with a spatial step equal to Δs.

In particular, the quasi-static component of the bed level and K values for flow depth are solved from downstream to upstream. Equation (C3) is applied at the downstream boundary of the model domain (say node M) to solve for $\bar{\eta}_L$. The K values for flow depth at node M are then computed given the hydrodynamic boundary conditions and the solution of $\bar{\eta}_L$.

After determining the dependent variables at the downstream boundary, the system of equations (C1) and (C2) is solved numerically. Here we discretize the equations using the Euler Forward method and a spatial step equal to Δs, but other explicit numerical methods can be applied too. The system of equations (C1) and (C2) is solved in a decoupled manner. This means that, with the flow conditions known at node M, equation (C2) computes the bed slope $\bar{S}$ at node M. Subsequently, the system of equation (C1) is used to compute the K values of flow depth at node M-1. Once the K values of flow depth at mode M-1 are known, the previous steps are repeated, resulting in a space-marching procedure in the upstream direction.

In the BWE model, we only solve the hydrodynamic equation through a space-marching method. The mathematical characteristics of this equation are different from the ones of the total system of ODEs of Model A. Consequently, the stability criterion differs between the backwater computation in the BWE model and the space-marching solution of Model A. In particular, it is the bed slope equation of Model A that requires a small spatial step.

Appendix D: The Numerical Solution of Model B

Model B of the dynamic component of the quasi-equilibrium state is described in Section 6. The numerical solution of Model B builds on the solution of the quasi-static component of the quasi-equilibrium state by Model A. It requires as input not only the solution of the quasi-static bed slope, $\overline{S}$, but also the flow variables such as the friction slope, S_f. Model B solves the bed-level fluctuations using the same spatial and temporal discretization as used in Model A.

Equation (10) is discretized using the Euler Forward method for the discretization in time and a first-order difference scheme for the discretization in space. This leads to

$$\Delta\eta(s^i, t^j) = \Delta\eta(s^i, t^{j-1}) + \Delta t\lambda(s^i, t^{j-1})\left(\overline{S}(s^i) - S_f(s^i, t^{j-1})\right), \tag{D1}$$

where $s^i = s_0 + i\Delta s$, where $1 \leq i \leq N$, Δs is the space step, and N is the number of grid cells.

The initial condition $\Delta\eta(s^i, t_0)$ is implicitly provided by the equilibrium condition in equation (3). A straightforward way to solve for bed-level fluctuation $\Delta\eta$ as a function of time is to first assume that $\widetilde{\Delta\eta}(s^i, t_0) = 0$ and solve equation (D1) to compute a time series of the dynamic component of the quasi-equilibrium state $\widetilde{\Delta\eta}(s^i, t^j)$ using this initial condition. Next, the solution is translated vertically to satisfy the condition regarding the mean bed-level fluctuation in equation (3). The solution of $\Delta\eta(s^i, t^j)$ follows from

$$\Delta\eta(s^i, t^j) = \widetilde{\Delta\eta}(s^i, t^j) - \overline{\widetilde{\Delta\eta}}(s^i). \tag{D2}$$

Appendix E: Numerical Settings

We test Models A and B against the time-marching numerical BWE model. The system of the BWE equations is a system of partial differential equations that is solved by marching through time.

For the runs with Models A and B, we use a time step, Δt, equal to 5 days. This yields $K = 365/5{*}100 = 7{,}300$ modes of the flow rate for the 100-year hydrograph. However, some of these modes are not unique, and we select $K = 2{,}289$ unique modes of the flow rate and solve a system of 2,290 ordinary differential equations (K backwater equations and one bed slope equation). The spatial step, Δs, is 10 m. This step is small with respect to the spatial scale of the problem, as a small spatial step is required for stability reasons when marching upstream.

The BWE model runs are made using the numerical research code Elv (e.g., Blom, Arkesteijn, et al., 2017; Blom, Chavarrías, et al., 2017; Chavarrías et al., 2018). It solves the equations in a decoupled manner (e.g., Blom, Arkesteijn, et al., 2017; Cao & Carling, 2002). It combines the same space-marching scheme for the hydrodynamic update as Model A (i.e., Euler forward) with an explicit Euler update for the bed-level update. We refer to Blom, Arkesteijn, et al. (2017) for additional details. The time step, Δt, is 5 days. The combination with a spatial step Δs of 1 km guarantees the CFL number to be smaller than 1.

The BWE model requires an initial condition, as well as a criterion for convergence to the equilibrium state. We impose the solution of the quasi-static component of the quasi-equilibrium state predicted by Model A as the initial condition in the BWE model runs. This significantly shortens the simulation time. The runs are continued for a total duration of 100,000 years, after which the difference in bed level before and after a cycled 100-year hydrograph is negligible, and we consider the computed state to be sufficiently close to the equilibrium state.

Acknowledgments
This research is part of the research program RiverCare, supported by the Dutch Technology Foundation TTW, which is part of the Netherlands Organization for Scientific Research (NWO), and which is partly funded by the Ministry of Economic Affairs under Grant P12-14 (Perspective Programme). The contribution by Matt Czapiga is funded through a TTW Water2015 project (Grant 14508, awarded to Blom). The model, input files, and model results are available at Zenodo (https://zenodo.org/record/3384198#.XW1cXPkzaUk). All data for this paper are cited and referred to in the reference list.

References

Ackers, P., & Charlton, F. G. (1970). Meander geometry arising from varying flows. *Journal of Hydrology*, *11*, 230–252. https://doi.org/10.1016/0022-1694(70)90064-8

Ahnert, F. (1994). Equilibrium, scale and inheritance in geomorphology. *Geomorphology*, *11*(2), 125–140. https://doi.org/10.1016/0169-555X(94)90077-9

An, C., Cui, Y., Fu, X., & Parker, G. (2017). Gravel-bed river evolution in earthquake-prone regions subject to cycled hydrographs and repeated sediment pulses. *Earth Surface Processes and Landforms*, *42*, 2426–2438. https://doi.org/10.1002/esp.4195

An, C., Fu, X., Wang, G., & Parker, G. (2017). Effect of grain sorting on gravel bed river evolution subject to cycled hydrographs: Bed load sheets and breakdown of the hydrograph boundary layer. *Journal of Geophysical Research: Earth Surface*, *122*, 1513–1533. https://doi.org/10.1002/2016JF003994

Barneveld, H. (1988). Numerieke methoden voor morfologische berekeningen tijdens kortdurende hoogwatergolven, Delft University of Technology. (in Dutch).

Blom, A., Arkesteijn, L., Chavarrías, V., & Viparelli, E. (2017). The equilibrium alluvial river under variable flow and its channel-forming discharge. *Journal of Geophysical Research: Earth Surface*, *122*, 1924–1948. https://doi.org/10.1002/2017JF004213

Blom, A., Chavarrías, V., Ferguson, R. I., & Viparelli, E. (2017). Advance, retreat, and halt of abrupt gravel-sand transitions in alluvial rivers. *Geophysical Research Letters*, *44*, 9751–9760. https://doi.org/10.1002/2017GL074231

Blom, A., Viparelli, E., & Chavarrías, V. (2016). The graded alluvial river: Profile concavity and downstream fining. *Geophysical Research Letters*, *43*, 6285–6293. https://doi.org/10.1002/2016GL068898

Bolla Pittaluga, M., Luchi, R., & Seminara, G. (2014). On the equilibrium profile of river beds. *Journal of Geophysical Research: Earth Surface*, *119*, 317–332. https://doi.org/10.1002/2013JF002806

Bolla Pittaluga, M., Tambroni, N., Canestrelli, A., Slingerland, R., Lanzoni, S., & Seminara, G. (2015). Where river and tide meet: The morphodynamic equilibrium of alluvial estuaries. *Journal of Geophysical Research: Earth Surface*, *120*, 75–94. https://doi.org/10.1002/2014JF003233

Cao, Z., & Carling, P. A. (2002). Mathematical modelling of alluvial rivers: Reality and myth. Part 2: Special issues. *Proceedings of the Institution of Civil Engineers Water & Maritime Engineering*, *154*(4), 297–307. https://doi.org/10.1680/wame.2002.154.4.297

Chatanantavet, P., & Lamb, M. P. (2014). Sediment transport and topographic evolution of a coupled river and river plume system: An experimental and numerical study. *Journal of Geophysical Research: Earth Surface*, *119*, 1263–1282. https://doi.org/10.1002/2013JF002810

Chatanantavet, P., Lamb, M. P., & Nittrouer, J. A. (2012). Backwater controls of avulsion location on deltas. *Geophysical Research Letters*, *39*, L01402. https://doi.org/10.1029/2011GL050197

Chavarrías, V., Stecca, G., & Blom, A. (2018). Ill-posedness in modelling mixed-sediment river morphodynamics. *Advances in Water Resources*, *114*, 219–235. https://doi.org/10.1016/j.advwatres.2018.02.011

Chorley, R. J., & Kennedy, B. A. (1971). *Physical geography: A systems approach*, pp. 370: Prentice Hall. https://doi.org/10.1002/qj.49709841818

Chow, V. T. (1959). *Open-Channel Hydraulics*. New York: McGraw-Hill.

Church, M. (2006). Bed material transport and the morphology of alluvial river channels. *Annual Review of Earth and Planetary Sciences*, *34*, 325–354. https://doi.org/10.1146/annurev.earth.33.092203.122721

De Vriend, H. (2015). The long-term response of rivers to engineering works and climate change. *Proceedings of the Institution of Civil Engineers*, *168*(CE3), 139–145. https://doi.org/10.1680/cien.14.00068

De Vries, M. (1965). Considerations about non-steady bed load transport in open channels (Tech. Rep. 36). The Netherlands: Delft Hydraulics Laboratory.

De Vries, M. (1971). Aspecten van zandtransport in open waterlopen (Tech. Rep.) Delft, Netherlands (in Dutch): Afd. der Weg- en Waterbouwkunde, Technische Hogeschool Delft.

De Vries, M. (1974). Sedimenttransport, Lecture Notes f10, Delft University of Technology, (in Dutch).

De Vries, M. (1975). A morphological time-scale for rivers. In *Proc XVIth IAHR congress*, São Paulo.

De Vries, M. (1993). Use of models for river problems, UNESCO.

Engelund, F., & Hansen, E. (1967). Monograph on sediment transport in alluvial streams (Tech. Rep.). Copenhagen, Denmark: Hydraul, Lab., Tech. Univ. of Denmark.

Exner, F. M. (1920). Zur Physik der Dünen. *Akademie der Wissenschaften, Wien, Mathematisch-Naturwissenschaftliche Klasse*, *129*(2a), 952. (in German).

Ferrer-Boix, C., Chartrand, S. M., Hassan, M. A., Martín-Vide, J. P., & Parker, G. (2016). On how spatial variations of channel width influence river profile curvature. *Geophysical Research Letters*, *43*, 6313–6323. https://doi.org/10.1002/2016GL069824

Frings, R., Banhold, K., & Evers, I. (2015). Sedimentbilanz des Oberen Rheindeltas für den Zeitraum 1991-2010 (Tech. Rep. 2015.019). Deutschland: Institut für Wasserbau und Wasserwirtschaft, RWTH Aachen. (in German).

Ganti, V., Chadwick, A. J., Hassenruck-Gudipati, H. J., Fuller, B. M., & Lamb, M. P. (2016). Experimental river delta size set by multiple floods and backwater hydrodynamics. *Science Advances*, *2*(5). https://doi.org/10.1126/sciadv.1501768

Gilbert, G. K. (1877). Report on the geology of the Henry Mountains, US Government Printing Office.

Howard, A. D. (1982). Equilibrium and time scales in geomorphology: Application to sand-bed alluvial streams. *Earth Surface Processes and Landforms*, *7*(4), 303–325. https://doi.org/10.1002/esp.3290070403

Lamb, M. P., Nittrouer, J. A., Mohrig, D., & Shaw, J. (2012). Backwater and river plume controls on scour upstream of river mouths: Implications for fluvio-deltaic morphodynamics. *Journal of Geophysical Research*, *117*(F01002). https://doi.org/10.1029/2011JF002079

Lane, E. W. (1955). The importance of fluvial morphology in hydraulic engineering. *Proceedings of the American Society of Civil Engineers*, *81*(754), 1–17.

Lane, E. W. (1957). A study of the shape of channels formed by natural streams flowing in erodible material (Tech. Rep.): US Army Corps of Engineers.

Lanzoni, S., Luchi, R., & Bolla Pittaluga, M. (2015). Modeling the morphodynamic equilibrium of an intermediate reach of the Po River (Italy). *Advances in Water Resources*, *81*, 95–102. https://doi.org/10.1016/j.advwatres.2014.11.004

Lauer, J. W., Viparelli, E., & Piegay, H. (2016). Morphodynamics and sediment tracers in 1-D (MAST-1D): 1-D sediment transport that includes exchange with an off-channel sediment reservoir. *Advances in Water Resources*, *93*, 135–149. https://doi.org/10.1016/j.advwatres.2016.01.012

Li, W., Wang, Z., de Vriend, H. J., & van Maren, D. S. (2014). Long-term effects of water diversions on the longitudinal flow and bed profiles. *Journal of Hydraulic Engineering*, *140*(6). https://doi.org/10.1061/(asce)hy.1943-7900.0000856

Mackin, J. H. (1948). Concept of the graded river. *Geological Society of America Bulletin*, *59*(5), 463–512. https://doi.org/10.1130/0016-7606(1948)59

Meade, R. H., Rayol, J. M., Da Conceicão, S. C., & Natividade, J. R. (1991). Backwater effects in the Amazon River basin of Brazil. *Environmental Geology and Water Sciences*, *18*(2), 105–114. https://doi.org/10.1007/BF01704664

Meyer-Peter, E., & Müller, R. (1948). Formulas for bed-load transport. In *Proc. 2nd Meeting Int. Assoc. Hydraul. Struct. Res.* (pp. 39–64) Stockholm.

Nittrouer, J. A., Mohrig, D., Allison, M. A., & Peyret, A.-P. B. (2011). The lowermost Mississippi River: A mixed bedrock-alluvial channel. *Sedimentology*, *58*(7), 1914–1934. https://doi.org/10.1111/j.1365-3091.2011.01245.x

Nittrouer, J. A., Shaw, J., Lamb, M. P., & Mohrig, D. (2012). Spatial and temporal trends for water-flow velocity and bed-material sediment transport in the lower Mississippi River. *Geological Society of America Bulletin*, *124*(3-4), 400–414. https://doi.org/10.1130/B30497.1

Paarlberg, A., Dohmen-Janssen, C. M., Hulscher, S., & Schielen, R. (2008). Modelling dynamic roughness in rivers during floods. In D. Parsons, T. Garlan, & J. Best (Eds.), *Marid 2008, 3rd Int. Workshop on Marine and River Dune Dynamics, Leeds, UK* (pp. 257–264). SHOM.

Paola, C. (2001). Modelling stream braiding over a range of scales, Gravel-Bed Rivers V. In M. P. Mosley (Ed.), *New Zealand Hydrological Society Inc.* (pp. 11–46). Wellington: New Zealand Hydrological Society Inc.

Paola, C., & Leeder, M. (2011). Environmental dynamics: Simplicity versus complexity. *Nature*, *469*, 38–39. https://doi.org/10.1038/469038a

Parker, G. (2004a). Morphodynamics of gravel-sand transitions, Chap. 27, *1D Sediment Transport Morphodynamics with Applications to Rivers and Turbidity Currents*: E-Book. http://hydrolab.illinois.edu/people/parkerg/morphodynamics&urluscore;e-book.htm

Parker, G. (2004b). Response of the gravel bed of a mountain river to a hydrograph. In *Proc. Int . Conf. on Slopeland Disaster Mitigation*, Taipei, Taiwan October 5–6.

Parker, G., Hassan, M. A., & Wilcock, P. (2008). Adjustment of the bed surface size distribution of gravel-bed rivers in response to cycled hydrograph. In H. Habersack, H. Piegay, & M. Rinaldi (Eds.), *Gravel-Bed Rivers VI: From Process Understanding to River Restoration* (pp. 241–285). https://doi.org/10.1016/S0928-2025(07)11127-5

Phillips, B. C., & Sutherland, A. J. (1989). Spatial lag effects in bed load sediment transport. *Journal of Hydraulic Research*, *27*(1), 115–133. https://doi.org/10.1080/00221688909499247

Pickup, G., & Rieger, W. A. (1979). A conceptual model of the relationship between channel characteristics and discharge. *Earth Surface Processes*, *4*(1), 37–42. https://doi.org/10.1002/esp.3290040104

Schielen, R. M. J., & Blom, A. (2018). A reduced complexity model of a gravel-sand river bifurcation: Equilibrium states and their stability. *Advances in Water Resources*, *121*, 9–21. https://doi.org/10.1016/j.advwatres.2018.07.010

Sinha, S. K., & Parker, G. (1996). Causes of concavity in longitudinal profiles of rivers. *Water Resources Research*, *32*, 1417–1428. https://doi.org/10.1029/95WR03819

Viparelli, E., Blom, A., & Parker, G. (2012). Modeling stratigraphy formed by prograding Gilbert-type deltas, River Flow 2012. In R. Murillo (Ed.), *Proc. Int. Conf. Fluvial Hydraulics* (pp. 827–836). London: CRC Press, Taylor and Francis Group.

Viparelli, E., Gaeuman, D., Wilcock, P., & Parker, G. (2011). A model to predict the evolution of a gravel bed river under an imposed cyclic hydrograph and its application to the Trinity River. *Water Resources Research*, *47*, W02533. https://doi.org/10.1029/2010WR009164

Viparelli, E., Lauer, J. W., Belmont, P., & Parker, G. (2013). A numerical model to develop long-term sediment budgets using isotopic sediment fingerprints. *Computers and Geosciences*, *53*, 114–122. https://doi.org/10.1016/j.cageo.2011.10.003

Wang, Z., Vries, M. D., Fokkink, R., & Langerak, A. (1995). Stability of river bifurcations in id morphodynamic models. *Journal of Hydraulic Research*, *33*(6), 739–750. https://doi.org/10.1080/00221689509498549

Wilcock, P. R., & Crowe, J. C. (2003). Surface-based transport model for mixed-size sediment. *Journal of Hydraulic Engineering*, *129*(2), 120–128. https://doi.org/10.1061/(ASCE)0733-9429(2003)129:2(120)

Wolman, M. G., & Miller, J. P. (1960). Magnitude and frequency of forces in geomorphic processes. *The Journal of Geology*, *68*(1), 54–74. https://doi.org/10.1086/626637

Wong, M., & Parker, G. (2006). *Journal of Geophysical Research*, *111*, F03018. https://doi.org/10.1029/2006JF000478

Zhou, Z., Coco, G., Townend, I., Olabarrieta, M., van der Wegen, M., Gong, Z., et al. (2017). Is "morphodynamic equilibrium" an oxymoron? *Earth-Science Reviews*, *165*, 257–267. https://doi.org/10.1016/j.earscirev.2016.12.002